IEICE TRANSACTIONS

on Electronics

This advance publication article will be replaced by the finalized version after proofreading.

Single-Layer Circular Polarizer for Linear Polarized Horn Antenna

Ryo KUMAGAI[†], **Student Member**, **Ryosuke SUGA**[†a)], **and Tomoki UWANO**[†], **Members**

SUMMARY In this paper, a single-layer circular polarizer for linear polarized horn antenna is proposed. The multiple reflected waves between the aperture and array provide desired phase differences between vertical and horizontal polarizations. The measured gain of the fabricated antenna is 14.4 dBic and the half power beamwidths of the vertical polarization are 28 and 24 deg. and those of the horizontal polarization are 31 and 23 degrees in the vertical and horizontal planes. The polarizer has a low impact on the gain and beamwidth of the primary horn antenna and their changes are within 1.7 dB and 10 degrees. The 3 dB fractional bandwidth of the axial ratio is measured to be 1.4 %.

key words: Circular polarization; horn antenna; element array; polarizer.

1. Introduction

The circular polarization has the advantages to avoid the multipath interference and polarization mismatch [1] [2]. Circular polarized antennas are used for a global positioning system [3], a reader for radio frequency identification [4], a satellite communication [5], a 5G system [6] and short-range communications [7]. A crossed dipole antenna [8], helical antenna [9], spiral antenna [10], microstrip patch antenna [11], slot antenna [12] are reported as the circular polarized antennas.

In comparison with these circular polarized antennas, arrangement of metal element arrays in front of a linearly polarized antenna aperture is effective in simplifying a feed network and reducing antenna size to convert linear to circular polarizations [13]. The equal amplitudes and phase differences of 90 degrees between the vertical and horizontal polarization are essential for the circular polarizer and they are are generally realized by using an orthogonal capacitive and inductive array. Polarizers using arrays of meander lines [14] - [16], split rings [17] - [19], cross slots [20], a lattice structure [21] - [23], and slabs [24] are reported so far. However, these polarizers require very thick or multiple arrays compared to the wavelength [26]. The authors had reported the feasibility study of the single-layer circular polarizer by using electromagnetic simulator [27] and its measurement evaluation [28]. However, the design of the polarizer had not been discussed.

In this paper, the optimal design of the single-layer circular polarizer for linear polarized horn antenna is discussed and its operation principle is also explained. The proposed
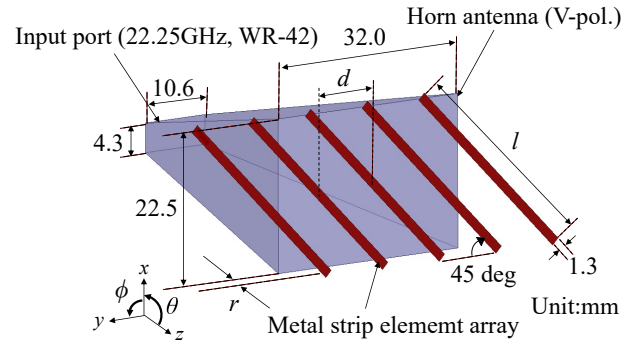
[†]The authors are with the Department of Electrical Engineering and Electronics, Aoyama Gakuin University.

a) E-mail: rsuga@ee.aoyama.ac.jp

Fig. 1 Structure of circularly polarized horn antenna.

polarizer convert linear to circular polarizartions in a single-layer element array and has pretty small impact for the gain and beamwidth of a primary linear polarized horn antenna. The required amplitude and phase difference are obtained by adjusting the distance between an antenna and the polarizer.

2. Proposed polarizer

Figure 1 shows the structure of a proposed polarizer with a linear polarized horn antenna. A vertically polarized rectangular horn antenna and a single-layer metal element array are used as the primary radiator (WR-42) and polarizer. The gain of the horn antenna is 16.1 dBi at 22.25 GHz. The circular polarization is obtained by combining the vertical and horizontal electric fields with appropriate amplitudes and phase differences. The significant difference of the reflection coefficient at the antenna aperture for both polarizations are applied to realize the required fields. Therefore, the square horn antenna is used as the primary radiator. The array with n elements is arranged in front of the antenna aperture with distance r and the elements have the tilt angle of 45 degrees to obtain the maximum horizontal polarization [29]. The element has the width of 1/10 wavelengths (1.3 mm) and length l and arrangement interval d. The rotational direction of the circularly polarization depends on the tilt direction of the elements and the antenna in Fig. 1 radiates the left-handed one.

Figure 2 shows the (a) vertical component and (b) horizontal component of the radiated electric field propagating $+z$ direction and these radiated electric field can be presented as

$$E_V e^{-jk_0 z} = E_{aV} e^{-jk_0 z} + E_{\Gamma V} e^{-jk_0 z} + E_0 e^{-jk_0 z} \quad (1)$$

$$E_H e^{-jk_0 z} = E_{aH} e^{-jk_0 z} + E_{\Gamma H} e^{-jk_0 z} \quad (2)$$

(a) Vertical component

E_{aH} is reflected due to cut-off of antenna.
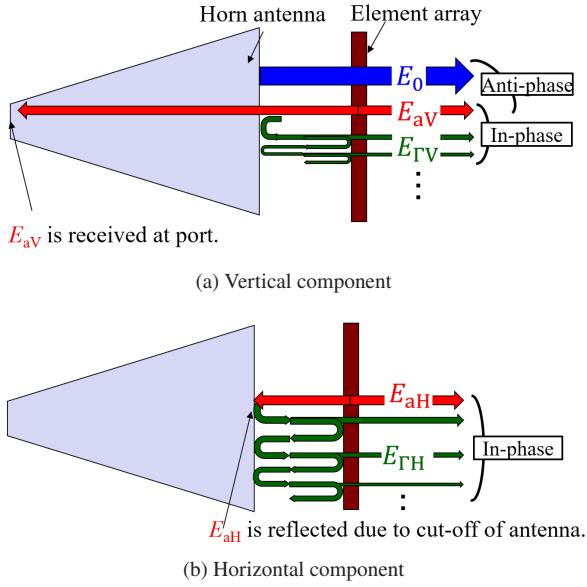
(b) Horizontal component

Fig. 2 Radiated electric field components.

Here, E_{aV} and E_{aH} are the radiated electric fields from the polarizer, $E_{\Gamma V}$ and $E_{\Gamma H}$ are those caused by the multiple reflected waves between the antenna aperture and the polarizer. E_0 is the radiated field from the primary horn antenna and k_0 is the wave number in the free space. All electric fields in both equations are obtained in the far-field at $\theta = 0$ degrees and $\phi = 90$ degrees. E_V and E_H are desired to have equal amplitude of $E_0/\sqrt{2}$. Thus, $E_{aV} + E_{\Gamma V}$ need to be anti-phase with E_0 to decrease E_V, and $E_{a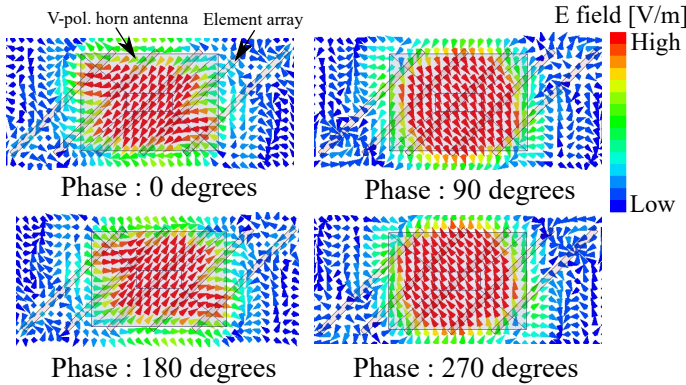H}$ and $E_{\Gamma H}$ should be in-phase to increase E_H. Thus, $E_{aV} + E_{\Gamma V}$ need to be anti-phase with E_0 to decrease E_V, and E_{aH} and $E_{\Gamma H}$ should be in-phase to increase E_H.

Fig. 3 Radiated electric field vectors at 22.25 GHz.

Figure 3 shows the simulated radiated electric field vectors on the observation plane at a distance of quater-wavelength away from the array. The figures are vectors viewed from - z to + z directions at 22.25 GHz and are simulated by using an electromagnetic simulator HFSS [30]. It is found that the vectors rotate with counter-clockwise and the left-handed circular polarization is obtained.
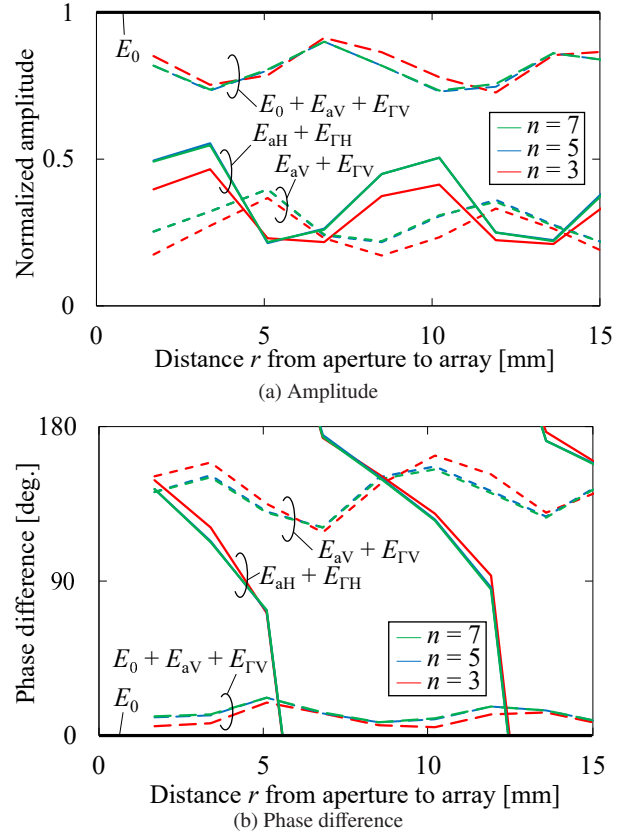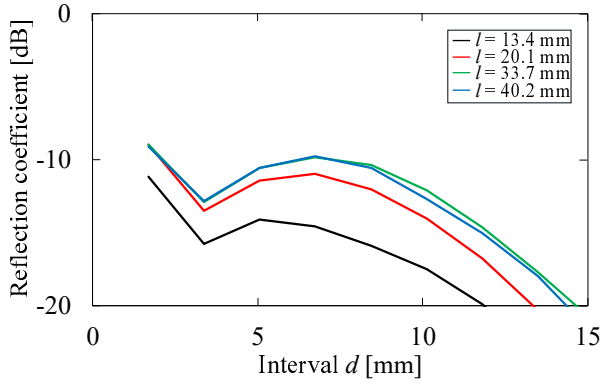

(a) Amplitude

(b) Phase difference

Fig. 4 Simulated distance r dependencies of the radiated electric fields with various n ($l = 33.7$ mm, $d = 10.1$ mm, 22.25 GHz).

3. Array design

3.1 Position r and number n of elements

Figure 4 shows the simulated distance r dependencies of the (a) amplitude and (b) phase difference of the vertical and horizontal components with various n. Here, the copper is used for the element array. $E_0 + E_{aV} + E_{\Gamma V}$ and $E_{aH} + E_{\Gamma H}$ are obtained by using electromagnetic field simulator. E_0 is also done by the simulation of the antenna without the array and $E_{aV} + E_{\Gamma V}$ is derived by subtracting E_0 from $E_0 + E_{aV} + E_{\Gamma V}$ as illustrated in Fig. 2. The desired conditions are as following; $|E_0 + E_{aV} + E_{\Gamma V}| = |E_{aH} + E_{\Gamma H}| = 1/\sqrt{2}$ and $\angle(E_{aH} + E_{\Gamma H})$ - $\angle(E_0 + E_{aV} + E_{\Gamma V}) = 90$ degrees. Note that the anti-phase between $E_{aV} + E_{\Gamma V}$ and E_0 are required to obtain the above amplitude condition. Here, $l = 5/2$ wavelengths (33.7 mm) as an example of the dimension longer than the aperture height of the antenna and $d = 3/4$ wavelengths (10.1 mm) to suppress grating lobes. Here, the amplitudes are normalized to that of the electric field E_0 radiated from the horn antenna and the reference value of the phase difference is the phase of E_0.
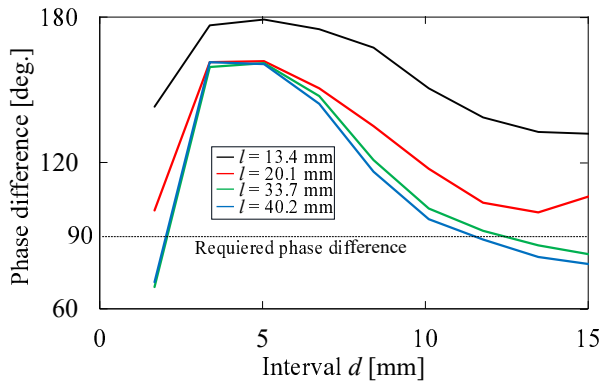
The amplitudes and phases are converged with $n \geq 5$ because the array is enough larger than the antenna aperture. All curves in the both figures are varied with the period of the half wavelength 6.8 mm. Both amplitude and phase

Fig. 5 Interval d dependence of reflection coefficient with various element length l ($n = 5$, $r = 3.4$ mm, 22.25 GHz).
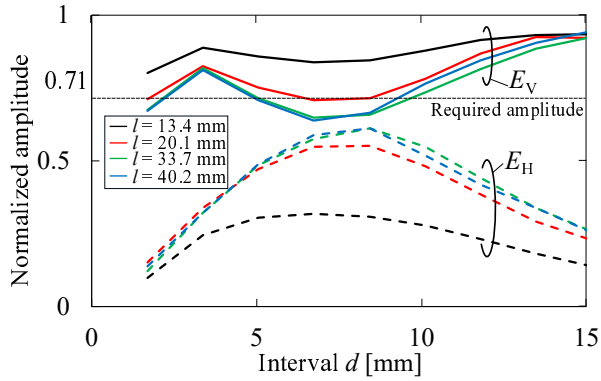

(a) Amplitude

(b) Phase difference

Fig. 6 Interval d dependence of radiated electric field with various element length l ($n = 5$, $r = 3.4$ mm, 22.25 GHz).

of horizontal components highly-depend on the distance r compared with those of the vertical ones. These are due to the reflection coefficient difference between the polarizations attributing the cut off characteristics of the feeding waveguide. The parameters of $r = 3.4$ mm and $n = 5$ provide the performances close to the above conditions; the maximum amplitude of $E_{aH} + E_{\Gamma H}$ of 0.55, the phase difference of 150 degrees between $E_{aV} + E_{\Gamma V}$ and E_0, and phase difference of 101 degrees between $E_{aH} + E_{\Gamma H}$ and $E_0 + E_{aV} + E_{\Gamma V}$.

3.2 Length l and interval d

The element length l and interval d are designed under the
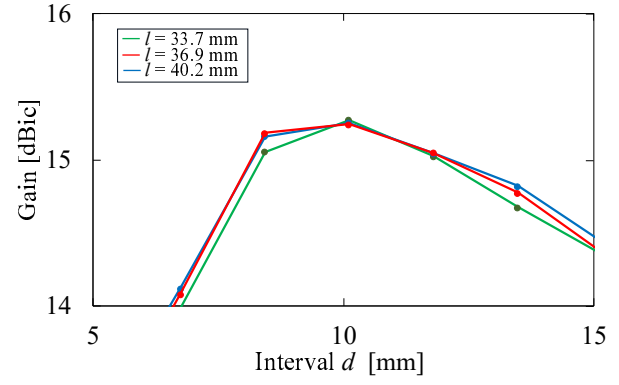

(a) Gain of circular polarization
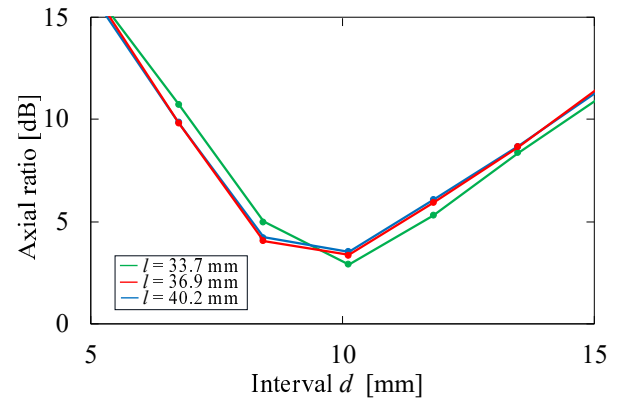
(b) Axial ratio

Fig. 7 Interval d of element dependence of each characteristic with various element length l ($n = 5$, $r = 3.4$ mm, 22.25 GHz).

conditions of $r = 3.4$ mm and $n = 5$. Here, the resolutions of d and l are 1/8 and 1/2 wavelengths. Figure 5 shows the simulated interval d dependencies of the reflection coefficient and the reflection below -10 dB are obtained with $d \geq 3.4$ mm. Figure 6 shows (a) amplitude and (b) phase difference between the vertical and horizontal poalrization. In the figure, the amplitudes in this figure is normalized to the electric field E_0 radiated from the horn antenna. The reflection and radiation characteristics are saturated with $l \geq 33.7$ mm because it is larger than the antenna aperture. The amplitude ratio less than 1.4 with phase difference of 90 degrees and the phase differences less than 110 degrees with the equal amplitude are required for 3 dB axial ratio. The conditions are obtained with $d = 10.1$ mm and 33.7mm $\leq l \leq 40.2$ mm. Figure 7 shows the simulated d dependencies of (a) circular polarization gain and (b) axial ratio under the above conditions. The maximum gain of 15.3 dBic and minimum axial ratio of 2.9 dB are obtained with $l = 33.7$ mm and $d = 10.1$ mm.

3.3 Improvement of axial ratio

The axial ratio of 2.9 dB is obtained at 22.25 GHz with the parameters of $r = 3.4$ mm, $n = 5$, $l = 33.7$ mm and $d = 10.1$ mm so far. In this section, the axial ratio will be improved by loading open stubs to the metal strip elements. Figure 8
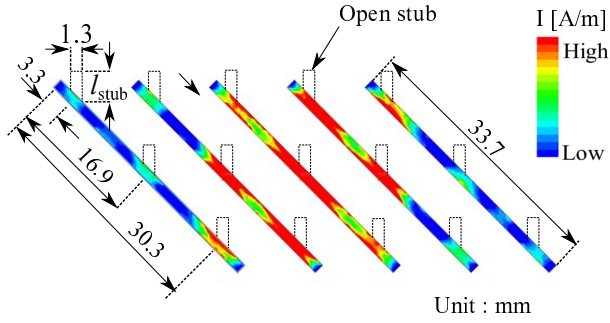
Fig. 8 Simulated surface current densities on the element array without stubs and the stubs positions (22.25 GHz).
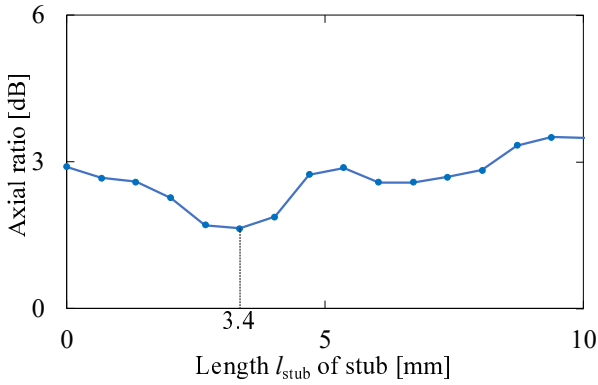
Fig. 9 Simulated axial ratio at 22.25 GHz against various l_{stub}.
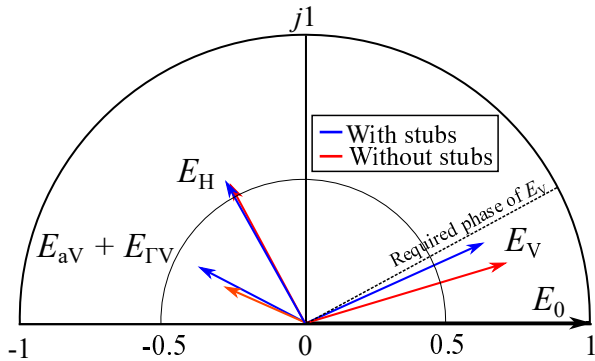
**Fig. 10** Simulated electric field vectors by adding the stubs with l_{stub} = 3.4 mm (22.25 GHz).

shows the simulated surface current densities on the element array and the stub positions. The high current densities are observed at 3.3, 16.9, and 30.3 mm from the element edge and the vertical open stubs with the dimensions of 1.3 mm $\times$ l_{stub} are added at the positions.

Figure 9 shows the simulated axial ratio at 22.25 GHz against various l_{stub}. The ratio with l_{stub} = 0 mm indicates the ratio without stubs. The minimum axial ratio of 1.4 dB is obtained with l_{stub} = 3.4 mm. Figure 10 shows the reactions of the simulated electric field vectors by adding the stubs with l_{stub} = 3.4 mm. Here, all vectors are normalized to E_0.

The stubs increase the amplitude of $E_{aV} + E_{\Gamma V}$ from 0.32 to 0.42 and have a low impact on E_H. The required phase difference of 90 degrees between E_V (= $E_0 + E_{aV} + E_{\Gamma V}$) and E_H with the stubs is indicated as a black dotted line. The amplitude of E_0 decrease from 0.73 to 0.68 because of increasing in the amplitude of $E_{aV} + E_{\Gamma V}$. Therefore the improvement of the axial ratio is owing to the change of E_V and the amplitude ratio and phase difference of E_V and E_H are improved to 1.2 and 94 degrees by attaching the stubs.

(a) Element array as polarizer

(b) Side view of polarizer and horn antenna
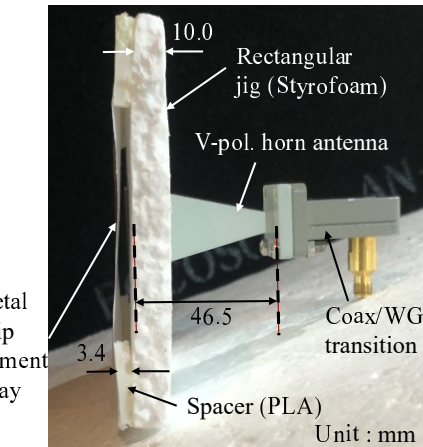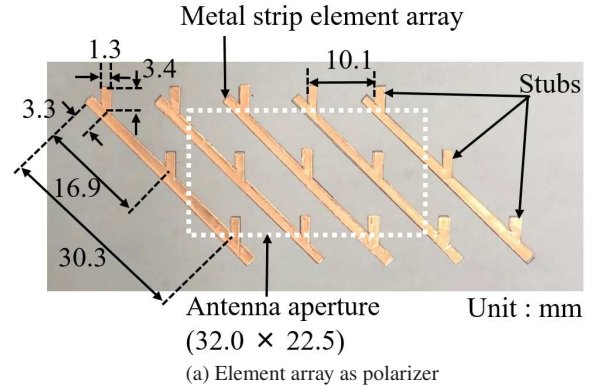
Fig. 11 Fabricated polarizer and linear polarized horn antenna.

4. Measurement

4.1 Axial ratio

Figure 11 shows the fabricated (a) element array as polarizer and (b) side view of polarizer and linear polarized horn antenna. The element array are made of copper tapes with their dimensions of 1.3 mm $\times$ 33.7 mm with the intervals of 10.1 mm and they are applied to a plain paper. The open stubs are connected at the 3.3, 16.9, and 30.3 mm from the element edge. A styrofoam plate with the thickness of 10.0 mm is fabricated and has a rectangular hole of the same dimensions as the horn antenna aperture, and the antenna is inserted into the plate hole. The antenna has the isometric dimensions of that in the simulation. To maintain the designed distance r =
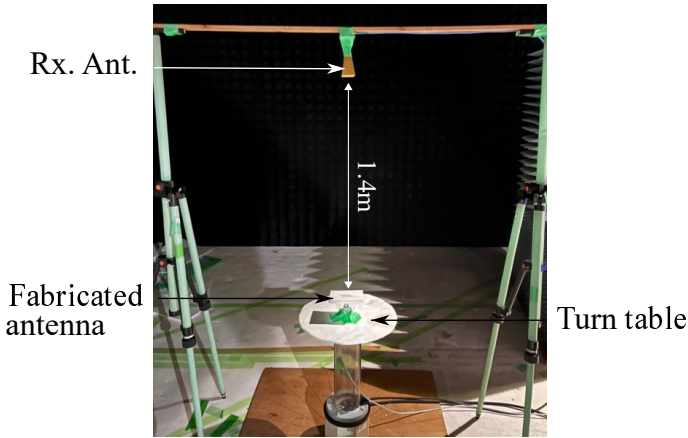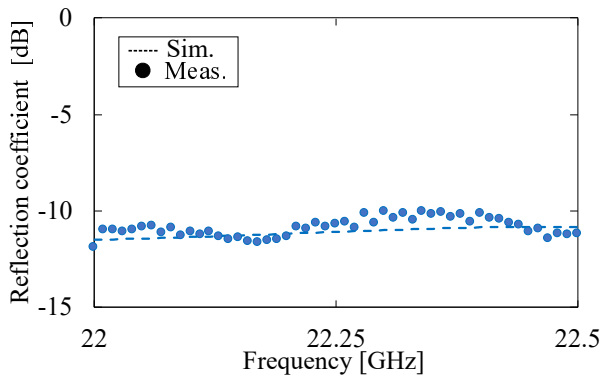
Fig. 12 Measurement system for axial ratio.

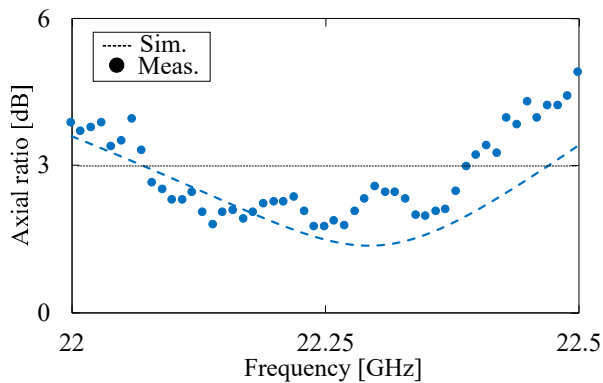**Fig. 13** Reflection coefficient.

Fig. 14 Frequency characteristics of the axial ratio.

3.4 mm, four plastic jigs are attached to the four corners of the styrofoam and the array is attached on the jigs.

Figure 12 shows the measurement system for the axial ratio of the fabricated antenna constructed in an anechoic chamber. The fabricated polarizer and horn antenna is placed toward upward direction on the center of the turn table to align the antenna and table axes. The receiving antenna was placed at 1.4 m high from the fabricated antenna using two tripod. The receiving antenna used is a linearly polarized horn antenna (WR-42) with the gain of 20 dBi at 22.25 GHz. In this measurement system, the turn table was rotated with

the resolution of 1 deg. and the transmission characteristics S_{21} were measured in the frequency from 22.0 GHz to 22.5 GHz. The axis ratio was calculated as the difference of the maximum and minimum S_{21} as following equation.

$$\text{Axial ratio [dB]} = \max(S_{21}) - \max(S_{21}) \tag{3}$$

Figure 13 shows the measured reflection coefficient of the fabricated polarizer. The reflection coefficient below -10 dB are obtained in the frequency range. Figure 14 shows the measured frequency characteristics of the axial ratio. The measured ratio agree with the simulated one within 1.1 dB and 1.7 dB is obtained at the center frequency of 22.25 GHz. The measured 3 dB fractional bandwidth of the axial ratio is 1.4%.

4.2 Radiation

Figures 15 and 16 show the radiation patterns for (a) E_V and (b) E_H at 22.25 GHz in the vertical (ϕ = 0 degrees.) and horizontal (ϕ = 90 degrees.) planes. The measured patterns of the primary horn antenna are also shown by the solid black lines. Note that the E_H components of the horn antenna are less than -40 dB. The measured mainlobes agree well with the simulated ones, and it is found that the element array does not have significant influences for the mainlobe of the horn antenna. Meanwhile, the measured sidelobe levels increased. The half power beamwidths are arranged in Table 1. The measured beamwidths of the vertical polarization are 28 and 24 deg. and those of the horizontal polarization are 31 and 23 degrees in the vertical and horizontal planes and their values agrees with simulated on within 6 degrees.

Figure 17 shows the measured frequency characteristics of the gains. The simulated gains at 22.25 GHz are 13.0 and 11.3 dBi for the E_V and E_H components. The latter is slightly small compared to the 3 dB down gain of the horn antenna, the gain is, however, adequate to achieve the axial ratio below 3 dB. The measured gains agreed with the simulated ones within 2.6 dB errors. The conductor loss of the array is confirmed as less than 0.05 dB by using the simulator and the differences between measured and simulated gains would be attributed to the fabrication error. The polarizer has a low impact on the gain and beamwidth of the primary horn antenna and their changes are within 1.7 dB and 10 degrees, respectively. The gain decreases are thought to be improved by sidelobe suppression.

Table 1 Half power Beamwidth at 22.25 GHz.

			Beamwidth [deg.]	
			ϕ = 0 deg.	ϕ = 90 deg.
Proposed polarizer	Sim.	E_V	32	28
		E_H	37	23
	Meas.	E_V	28	24
		E_H	31	23
Horn antenna	Meas.	E_V	28	29
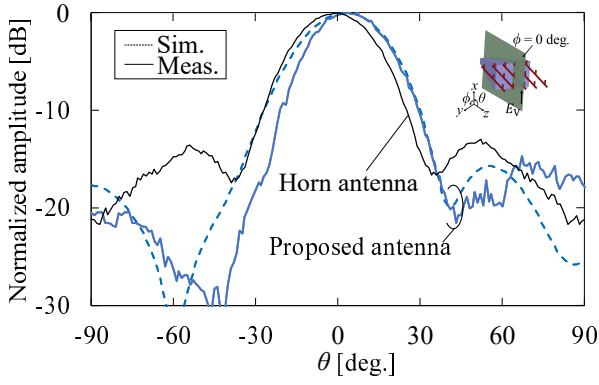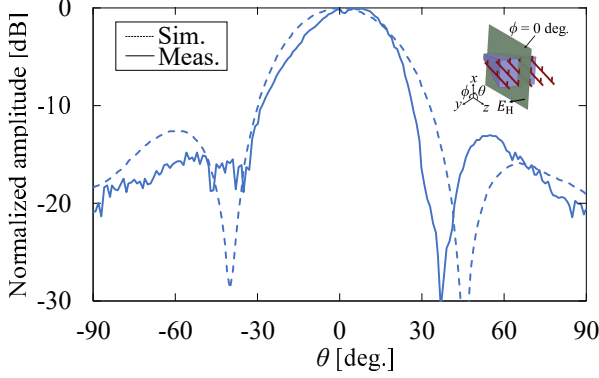
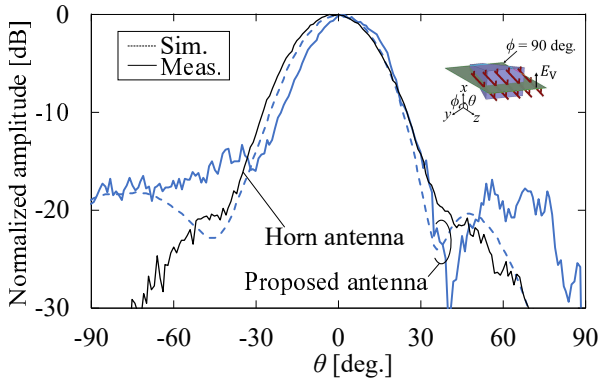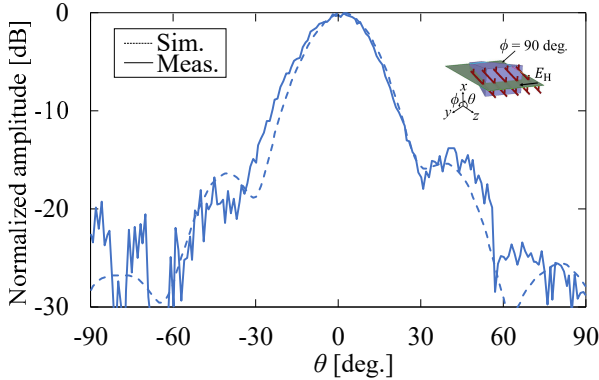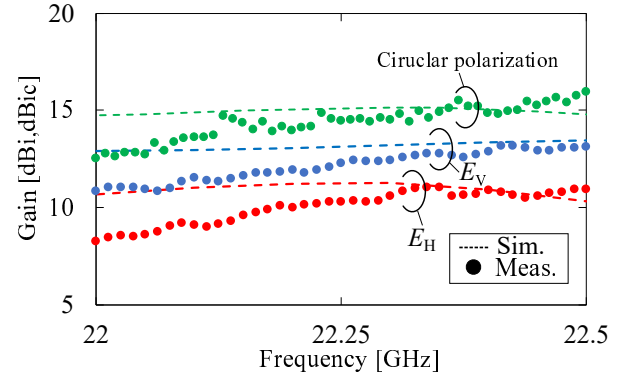**Fig. 15**   Radiation pattern in $\phi = 0$ degrees. plane (22.25 GHz).

Fig. 16   Radiation pattern in $\phi = 90$ degrees. plane (22.25 GHz).

Fig. 17   Frequency characteristics of the gain.

5.   Conclusion

In this paper, a single-layer circular polairzer for a linear polarized horn antenna is proposed. A vertically polarized rectangular horn antenna and a single-layer metal element array are used as the primary radiator and polarizer. The required conditions between the vertical and horizontal electric field can be achieved by the multiple reflection between the antenna aperture and the array. The polarizer has a low impact on the gain and beamwidth of the primary horn antenna and their changes are within 1.7 dB and 10 degrees. The sidelobe level suppression is an issue to be addressed in the future.

References

[1] S. X. Ta, and I. Park, "Crossed dipole loaded with magneto-electric dipole for wideband and wide-beam circularly polarized radiation," *IEEE Antennas Wireless Propag. Lett.*, vol. 14, pp. 358-361, Oct. 2014.

[2] M. Li and K. -M. Luk, "A Wideband Circularly Polarized Antenna for Microwave and Millimeter-Wave Applications," *IEEE Trans. Antennas Propag.*, vol. 62, no. 4, pp. 1872-1879, April 2014.

[3] O. P. Falade, M. U. Rehman, Y. Gao, X. Chen, and C. G. Parini, "Single feed stacked patch circular polarized antenna for triple band GPS receivers," *IEEE Trans. Antennas Propag.*, vol. 60, no. 10, pp. 4479-4484, Oct. 2012.

[4] R. Cao and S. -C. Yu, "Wideband compact CPW-Fed circularly polarized antenna for universal UHF RFID reader," *IEEE Trans. Antennas Propag.*, vol. 63, no. 9, pp. 4148-4151, Sep. 2015.

[5] S. Mener, R. Gillard, and L. Roy, "A dual-band dual-circular-polarization antenna for Ka-band satellite communications," *IEEE Antennas Wireless Propag. Lett.*, vol. 16, pp. 274-277, May 2016.

[6] Q. Wu, J. Hirokawa, J. Yin, C. Yu, H. Wang, and W. Hong, "Millimeter-wave multibeam endfire dual-circularly polarized a antenna array for 5G wireless applications," *IEEE Trans. Antennas Propag.*, vol. 66, no. 9, pp. 4930-4935, Sep. 2018.

[7] H. Aissat, L. Cirio, M. Grzeskowiak, J. M. Laheurte, and O. Picon, "Reconfigurable circularly polarized antenna for short-range communication systems," *IEEE Trans. Microw. Theory Tech.*, vol. 54, no. 6, pp. 2856-2863, June 2006.

[8] Y. He, W. He, and H. Wong, "A wideband circularly polarized cross-dipole antenna," *IEEE Antennas Wireless Propag. Lett.*, vol. 13, pp. 67-70, Jan. 2014.

[9] C. Liu, Y. -X. Guo, and S. Xiao, "Circularly polarized helical antenna for ISM-band ingestible capsule endoscope systems," *IEEE Trans. Antennas Propag.*, vol. 62, no. 12, pp. 6027-6039, Dec. 2014.

[10] N. Ghassemi, K. Wu, S. Claude, X. Zhang, and J. Bornemann, "Compact coplanar waveguide spiral antenna with circular polarization for wideband applications," *IEEE Trans. Antennas Wireless Propag. Lett.*, vol. 10, pp. 666-669, June 2011.

[11] Nasimuddin, X. Qing, and Z. N. Chen, "Compact asymmetric-slit microstrip antennas for circular polarization," *IEEE Trans. Antennas Propag.*, vol. 59, no. 1, pp. 285-288, Nov. 2010.

[12] Kin-Lu Wong, Chien-Chin Huang, and Wen-Shan Chen, "Printed ring slot antenna for circular polarization," *IEEE Trans. Antennas Propag.*, vol. 50, no. 1, pp. 75-77, Jan. 2002.

[13] W. Li, S. Gao, and Y. Cai, "Polarization-Reconfigurable Circularly Polarized Planar Antenna Using Switchable Polarizer," *IEEE Trans. Antennas Propag.*, vol. 65, no. 9, pp. 4470-4477, Sept. 2017.

[14] M. A. Joyal and J. J. Laurin, "Analysis and design of thin circular polarizers based on meander lines," *IEEE Trans. Antennas Propag.*, vol. 60, no. 6, pp. 3007-3011, Apr. 2012.

[15] M. N. Iqbal, M. F. M. Yusoff, M. K. A. Rahim, M. R. Bin Hamid, Z. Johari, and H. U. Rahman, "Circularly polarized transmitarray antenna design using meander line polarizer for Ku-band applications," *IEEE Access*, vol. 9, pp. 119598-119612, Aug. 2021.

[16] M. A. Joyal, M. Riel, Y. Demers, and J. J. Laurin, "A meander-line circular polarizer optimized for oblique incidence," *IEEE Trans. Antennas Propag.*, vol. 63, no. 12, pp. 5391-5398, Dec. 2015.

[17] L. Martinez-Lopez, J. Rodriguez-Cuevas, J. I. Martinez-Lopez, and A. E. Martynyuk, "A multilayer circular polarizer based on bisected split-ring frequency selective surfaces," *IEEE Antennas Wireless Propag. Lett.,* vol. 13, pp. 153-156, Jan. 2014.

[18] F. A. Mangi, S. Xiao, and Q. A. Arain, "Asymmetric Fission Transmission of Linear-to-Circular Polarization Converter Using Bi-layer Split Ring Structure." *Wireless Pers. Commun.*, vol.99, pp. 985–997 Dec. 2018.

[19] Y. Cheng, R. Gong, Z. Cheng, and Y. Nie, *Applied Optics*, vol. 53, pp. 5763-5768, 2014.

[20] J. Lundgren, O. Zetterstrom, F. Mesa, N. J. G. Fonseca, and O. Quevedo-Teruel, "Fully metallic dual-band linear-to-circular polarizer for K/Ka-band," *IEEE Antennas Wireless Propag. Lett.,* vol. 20, no. 11, pp. 2191-2195, Nov. 2021.

[21] H. Li, B. Li, and L. Zhu, "Wideband Linear-to-Circular Polarizer Based on Orthogonally Inserted Slot-Line Structures," *IEEE Antennas Wireless Propag. Lett.*, vol. 18, no. 6, pp. 1169-1173, June. 2019.

[22] B. Lin, J. Guo, Y. Wang, Z. Wang, B. Huang, and X. Liu, "A Wide-Angle and Wide-Band Circular Polarizer Using a BI-Layer Metasurface", *Progress In Electromagnetics Research*, vol. 161,pp. 125-133, May. 2018.

[23] X. Gao, K. Li, X. Wu, C. Xue, G. Wang, X. Xie, and M. Qin, "Ultra-wideband linear-to-circular polarizer realized by bi-layer metasurfaces", *Optics Express*, vol. 30, pp. 18392-18401, 2022.

[24] M. Akbari, M. Farahani, A. -R. Sebak, and T. A. Denidni, "Ka-Band Linear to Circular Polarization Converter Based on Multilayer Slab With Broadband Performance," *IEEE Access*, vol. 5, pp. 17927-17937, Aug. 2017.

[25] K. X. Wang and H. Wong, "A Wideband Millimeter-Wave Circularly Polarized Antenna With 3-D Printed Polarizer," *IEEE Trans. Antennas Propag.*, vol. 65, no. 3, pp. 1038-1046, Mar. 2017.

[26] J. D. Baena, S. B. Glybovski, J. P. del Risco, A. P. Slobozhanyuk and P. A. Belov, "Broadband and Thin Linear-to-Circular Polarizers Based on Self-Complementary Zigzag Metasurfaces," *IEEE Trans. Antennas and Propag.*, vol. 65, no. 8, pp. 4124-4133, Aug. 2017.

[27] U. Nakazawa, R. Suga, T. Uwano, "A Study on Phase Improvement on Radiated Electric Field from Circularly Polarized Horn Antenna Using Parasitic Elements", *IEICE Technical Report*, vol. 120, no. 328, EST2020-63, pp. 56-61, Jan. 2021. (In Japanese)

[28] R. Kumagai, S. Nakano, T. Uwano, and R. Suga, "Experimental study on circularly polarized horn antenna using parasitic element array," *2022 Asia-Pacific Microw. Conf.*, TH3-F3-5, pp. 405-407, Dec. 2022.

[29] Ruey-Shi Chu and Kuan-Min Lee, "Analytical method of a multi-layered meander-line polarizer plate with normal and oblique plane-wave incidence," *IEEE Trans. Antennas Propag.*, vol. 35, no. 6, pp. 652-661, June 1987.

[30] ANSYS HFSS, Available: https://www.ansys.com/ja-jp/products/electronics/ansys-hfss, reference, June 2022.

Ryo Kumagai received B.E degrees in Electrical Engineering and Electronics from Aoyama Gakuin University, Kanagawa, Japan in 2020. He is currently a master course student in the Department of Electrical Engineering and Electronics, Aoyama Gakuin University. He has been engaged in research on electromagnetic field simulation for antenna.

Ryosuke Suga received his B.E., M.E. and D.E. degrees in electrical engineering and electronics from Aoyama Gakuin University, Kanagawa, Japan in 2002, 2004 and 2008, respectively. He was a postdoctral research fellow at Tokyo Institute of Technology from 2008 to 2010. He was a research assistant at Aoyama Gakuin University in 2011 and an assistant professor from 2012 to 2021. He is an associate professor there. He has been engaged in research on microwave and millimeter-wave passive circuits, antennas and EMC. He is a member of the Institute of Electrical and Electronics Engineers (IEEE) and the Institute of Electrical Engineers of Japan (IEEJ). He received IEEE MTT-S Japan Chapter Young Engineer Award and IEICE Trans. Communications best paper award in 2013.

Tomoki Uwano received his B.E. degrees from the Tokyo Institute of Technology in 1971 and his Doctor of Engineering degrees from Osaka University in 1994. In 1971 he joined Matsushita Elect. Ind. Co. Ltd. (currently Panasonic), Osaka, Japan, where he has been engaged in research and development on microwave and mm-wave circuitry, and satellite and cellular radio communications. From April 1985 to December 1986, he was a visiting scholar in the department of electrical and computer engineering of theUniversity of Texas atAustin. From 2003 to 2015, hewas a visiting professor in the graduate school of information, production and systems of Waseda University, and since 2009 he has been a visiting research instructor in the college of science and engineering of Aoyama Gakuin University.